

ZOOMING IN ON THE COMA CLUSTER WITH *CHANDRA*: COMPRESSED WARM GAS IN THE BRIGHTEST CLUSTER GALAXIES

A. VIKHLININ, M. MARKEVITCH, W. FORMAN, AND C. JONES
Harvard-Smithsonian Center for Astrophysics, 60 Garden St., Cambridge, MA 02138;
avikhlinin@cfa.harvard.edu
Submitted to *ApJ Letters*, February 27 2001

ABSTRACT

The *Chandra* image of the central region of the Coma cluster reveals that both its dominant galaxies, NGC 4874 and NGC 4889, retain the central parts of their X-ray gas coronae. The interstellar gas with a temperature of 1–2 keV is confined by the hot intergalactic medium of the Coma cluster into compact clouds (only 3 kpc in radius) containing $10^8 M_{\odot}$ of gas. The physical state of the gas in these clouds appears to be determined by a delicate balance between radiative cooling and suppressed (by a factor of 30–100) heat conduction through the interface between these clouds and the hot cluster gas.

Subject headings: galaxies: clusters: general — galaxies: clusters: individual (Coma) — magnetic fields — X-rays: galaxies — galaxies: individual (NGC 4874) — galaxies: individual (NGC 4889)

1. INTRODUCTION

ROSAT observations showed that the Coma cluster, once thought to be an archetype of a relaxed system, contains substructures on a wide range of linear scales (Briel, Henry & Böhringer 1992, White, Briel & Henry 1993, Vikhlinin, Forman & Jones 1997). The detected structures include 100 kpc-scale X-ray enhancements around the two dominant cluster galaxies, NGC 4874 and NGC 4889 (Vikhlinin, Forman, & Jones 1994). Recent XMM observations confirmed these findings and also revealed unresolved X-ray sources coincident with these galaxies (Arnaud et al. 2001, Briel et al. 2001). In this *Letter*, we resolve these sources with *Chandra*. Both sources are extended arcsec-scale (≈ 3 kpc) remnants of galactic X-ray coronae with temperatures 1–2 keV, compressed by the hot, 9 keV, gas of the Coma cluster. Their very existence poses interesting physical questions.

The problem of thermal evaporation of cold clouds embedded in a hot medium has been considered in a number of papers (Cowie & McKee 1977, McKee & Cowie 1977, Balbus & McKee 1982, McKee & Begelman 1990, Bandiera & Chen 1994 among others). This problem is relevant for the survival of cold clouds in multi-phase cluster cooling flows (e.g., Böhringer & Fabian 1989, Fabian, Canizares, & Böhringer 1994). The general consensus emerging from these studies, as summarized by Fabian (1994), is that heat conduction must be suppressed by one to two orders of magnitude below the Spitzer value, otherwise the radiative cooling of the gas will be overcome by heat conduction. However, the direct evidence for suppression of heat conductivity in the intracluster medium (ICM) is scarce (one of a few examples can be found in Bechtold et al. 1983). The *Chandra* observations of the interstellar medium in the Coma galaxies presented here allow a direct study of cold clouds embedded in a hot intracluster medium.

We use $H_0 = 50 \text{ km s}^{-1} \text{ kpc}^{-1}$, which implies a linear scale of 0.68 kpc per arcsec at the Coma distance ($d = 140 \text{ Mpc}$).

2. *CHANDRA* OBSERVATIONS

The Coma cluster was observed with ACIS in the fall of 1999 in a series of 6 pointings with individual exposures of 10 ksec. The pointing position was kept the same during these observations, with NGC 4874 and NGC 4874 located at off-axis dis-

tances of 2.8' and 4.0', respectively. The detector was moved in the focal plane between the pointings, so that the galaxies were observed by both ACIS-I (4 times) and ACIS-S (2 times). There were no background flares in the Coma observations. In one pointing, NGC 4874 was located in the gap between the ACIS-I chips. The total exposure was 48 ksec for NGC 4874 and 56 ksec for NGC 4889.

The central part of the composite ACIS-I image is shown in Fig. 1. Notice the faint arcmin-scale X-ray enhancements around NGC 4874 and 4889, previously detected by *ROSAT*. At the center of these extended structures there are bright (500 counts) compact sources coincident with the optical positions of the galaxies. The observed 0.5–2 keV flux is $3.9 \pm 0.1 \times 10^{-14} \text{ erg s}^{-1} \text{ cm}^{-2}$ for NGC 4874 and $3.2 \pm 0.1 \times 10^{-14} \text{ erg s}^{-1} \text{ cm}^{-2}$ for NGC 4889, corresponding to luminosities in the same band of 9.1×10^{40} and $7.6 \times 10^{40} \text{ erg s}^{-1}$.

The enlarged X-ray and optical images of NGC 4874 and 4889 are shown in Fig. 2. The X-ray sources associated with the galaxies are extended, but unlike most ellipticals, the X-ray emission is much more compact than the distribution of optical light. Below we discuss these interesting objects in detail.

3. SPECTRAL ANALYSIS

The spectra of the NGC 4874 and 4889 sources were extracted within a radius of 7'' (which encompasses most of the observed X-ray flux). Since we are interested in the intrinsic properties of the galaxies, we collected the background spectra in the 15''–30'' annuli around them, so it includes the true background as well as the emission of the Coma cluster. The source, background spectra, and the response files were generated individually for each pointing. We then co-added the observed spectra and averaged the response files for each source.

In the spectra for both galaxies (Fig. 2), one immediately notices strong emission lines near 1 keV — a key signature of a 1 keV-temperature plasma. Indeed, the spectra are well fit by the Mewe-Kaastra-Liedahl model in XSPEC with the absorption fixed at the Galactic value $N_H = 9 \times 10^{19} \text{ cm}^{-2}$. Therefore, the observed X-ray emission is most likely produced by warm interstellar gas. The X-ray emission cannot be due to the integrated emission of stars because its spatial distribution does not follow the optical light (Fig. 2 and 4). Any significant

contribution by low-mass X-ray binaries (LMXB) can be ruled out because it also should follow the starlight and have a very different (hard) spectrum (Sarazin, Irwin, & Bregman 2001).

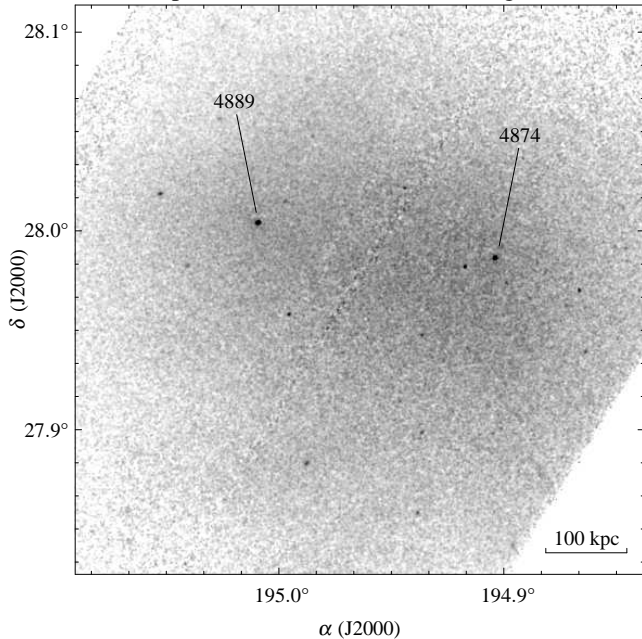


FIG. 1.— The central region of the composite exposure-corrected ACIS-I image of Coma in the 0.5–2 keV energy band. The narrow band running from bottom-left to top-right is the chip gap; it disappears in the smoothed image.

The best-fit temperatures and metal abundances of these sources are listed in Table 1 (the uncertainties hereafter are at the 68% confidence level for one interesting parameter). The average temperature is 1.0 keV for NGC 4874 and 1.8 keV for NGC 4889. The average abundance of heavy elements is close to the Solar value in both galaxies. This is significantly higher than the metal abundance in the surrounding Coma gas (0.25 ± 0.02 , Arnaud et al. 2001).

Chandra's angular resolution permits spectral fitting in several concentric annuli in NGC 4874. This analysis reveals a marginally significant (at the 99% confidence level) decrease of the gas temperature towards the center of the galaxy (Fig. 3 and Table 1). NGC 4889 does not show any non-isothermality, but the statistical errors are much larger.

TABLE 1
SPECTRAL RESULTS

Object	kT (keV)	a (Solar)	$\chi^2/\text{d.o.f}$
NGC 4874	1.00 ± 0.04	$0.79^{+0.84}_{-0.22}$	23.5/16
NGC 4874 ($0''$ – $1.5''$)	0.85 ± 0.06	0.79^*	16.5/17
NGC 4874 ($1.5''$ – $4''$)	1.11 ± 0.08	0.79^*	14.1/17
NGC 4889	$1.82^{+0.22}_{-0.10}$	$1.3^{+\infty}_{-0.4}$	17.9/16

* — fixed.

The errorbars are at the 68% confidence level for one interesting parameter. The 90% lower limit on the average metal abundance is 0.43 and 0.81 for NGC 4874 and NGC 4889, respectively.

We also checked for a possible fall in the projected temperature of the main cluster emission on an arcmin scale around the galaxies, as observed by XMM around NGC 4874 (Arnaud et al. 2001). We find no indication for cool gas beyond the small radius of the galactic sources. In the $10''$ – $1'$ annuli centered on the galaxies, we measure $T = 8.9 \pm 0.4$ and 9.2 ± 0.4 keV for NGC 4874 and 4889, respectively; these temperatures are con-

sistent with *Chandra* and *XMM* temperatures farther away, in the $1'$ – $3'$ annuli around the galaxies.

4. SPATIAL DISTRIBUTION OF THE INTERSTELLAR GAS

The X-ray surface brightness profile of NGC 4874 is shown in Fig. 4. A comparison with the point source profile (dotted line) clearly shows that the observed X-ray emission is extended. We fit the observed profiles with the β -model, $n_e = n_0(1 + r^2/r_c^2)^{-3\beta/2}$, truncated at some radius, r_{cut} , which is also a free parameter. The truncation of the gas distribution at r_{cut} is required because the ISM is embedded in the high-pressure cluster gas and, obviously, cannot extend beyond the radius at which the internal and external pressures are equal. The distribution of volume emissivity was computed assuming a constant temperature for NGC 4889 and the observed temperature gradient for NGC 4874 (Fig. 3).

We had to account for the *Chandra* PSF in fitting the surface brightness profiles because the source size is comparable to that of the PSF. The PSF model was obtained from the library of raytracing simulations; the PSF model is consistent with the image of the point source located $\approx 1'$ East of NGC 4874.

TABLE 2
GAS DENSITY DISTRIBUTION PARAMETERS

Object	n_{e0} , cm^{-3}	r_c , kpc	β	r_{cut} , kpc
NGC 4874	0.18 ± 0.02	0.8 ± 0.3	0.5^*	2.7 ± 0.4
NGC 4874, no cut	0.14 ± 0.02	2.4 ± 0.7	$1.8^{+0.5}_{-0.5}$...
NGC 4889	0.09 ± 0.01	2.0 ± 0.7	0.5^*	3.1 ± 0.3
NGC 4889, no cut	0.10 ± 0.01	3.3 ± 0.7	$1.7^{+0.5}_{-0.5}$...

* — fixed.

The results of the surface brightness profile modeling are summarized in Table 2. We were unable to obtain meaningful constraints on β because of the parameter correlation and finite PSF. Generally, all $\beta > 0.4$ are allowed. The cutoff and core-radii are well-constrained for $\beta < 1$. For larger β , the cutoff radius becomes much larger than the core-radius and hence has almost no effect on the observed profile. For a pure β -model without a cutoff, β must be in excess of 1.2–1.3, mimicking the cutoff at $1r_c - 2r_c$, which is consistent with the best-fit r_{cut} . Of course, different models correspond to very similar absolute gas density distributions in the radial range of interest.

5. DISCUSSION

5.1. Pressure Equilibrium of ISM and Cluster Gas

It is interesting to compare the pressure of the ISM at the best-fit cutoff radius with the external pressure of the cluster gas. Even though the three-dimensional location of the galaxies within the cluster is uncertain, the ICM density in their vicinity can be determined rather accurately because each galaxy has an associated arcmin-scale X-ray enhancement (Vikhlinin et al. 1994): $n_{\text{icm}} = 2.9 \times 10^{-3} \text{ cm}^{-3}$ around NGC 4874 and $5.7 \times 10^{-3} \text{ cm}^{-3}$ around NGC 4889. The temperature of the cluster gas around both galaxies is $T_{\text{icm}} = 9$ keV (see above). Remarkably, we find that for the observed ISM parameters, the pressure ratio at $r = r_{\text{cut}}$ is $p_{\text{ism}}/p_{\text{icm}} = 1.1 \pm 0.3$ for NGC 4874 and 1.2 ± 0.3 for NGC 4889. Therefore, the pressure of the ISM in both galaxies equals the external pressure at a radius where the *Chandra* image independently indicates an ISM density cutoff. This is a clear indication that the distribution of the ISM is

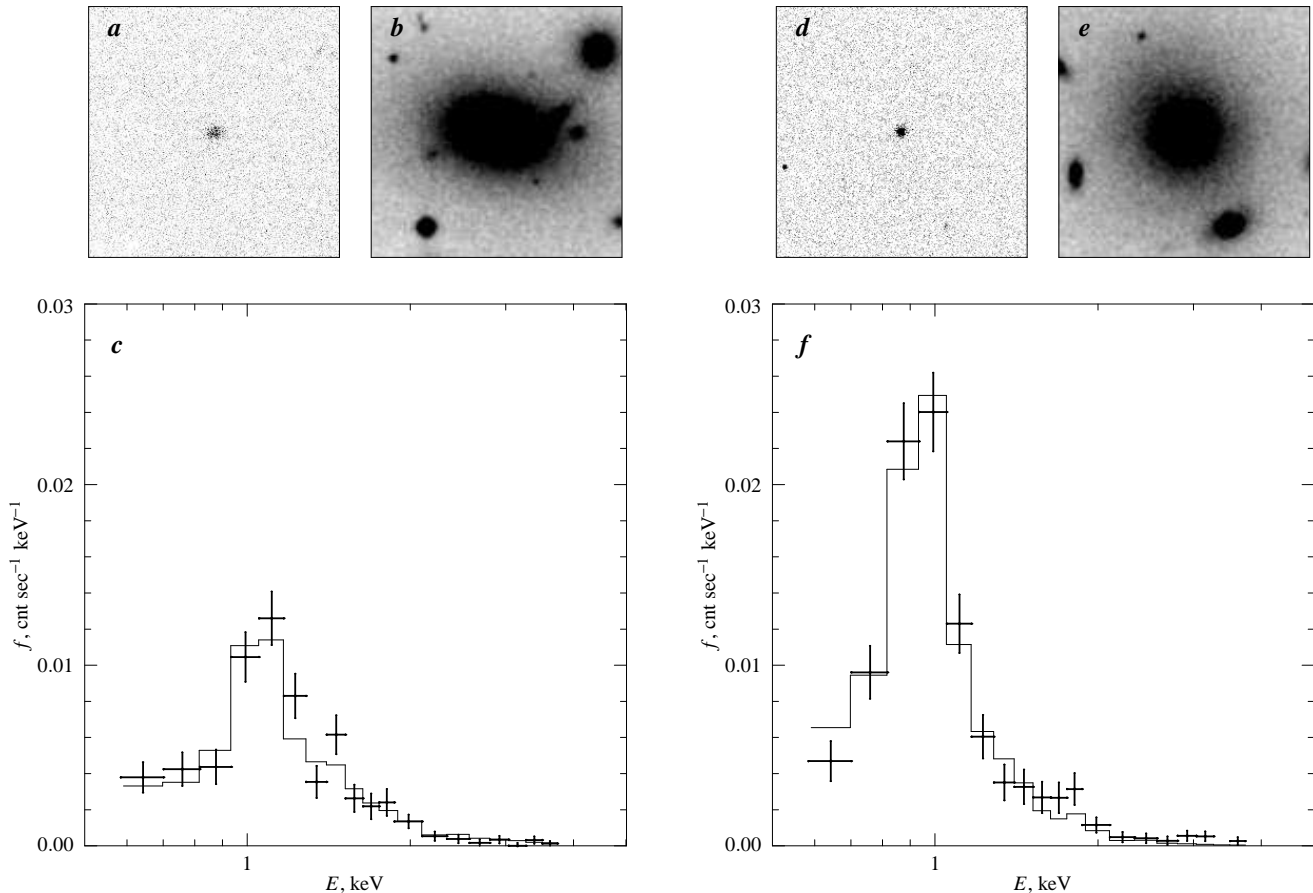


FIG. 2.— Images and spectra of NGC 4889 (*a, b, c*) and NGC 4874 (*d, e, f*). The X-ray (0.5–2 keV) and optical images have the same angular size, $2' \times 2'$. Solid histograms in panels *c* and *f* show the best-fit model with parameters from Table 1.

affected by the external pressure. The derived central ISM densities are higher by a factor of 2–10 than those normally found in isolated elliptical galaxies ($n_0 = 0.01 - 0.06 \text{ cm}^{-3}$; Forman, Jones & Tucker 1985), which also suggests compression by an external pressure.

5.2. Origin and Lifetime Scales for the ISM

Stellar ejecta is the most likely source of interstellar gas since the metal abundance in the ISM of both galaxies is significantly higher than that in the Coma ICM. The observed gas mass ($1.1 \pm 0.1 \times 10^8 M_\odot$ and $1.6 \pm 0.3 \times 10^8 M_\odot$ in NGC 4874 and NGC 4889, respectively) would be ejected by stars over the time $t_* = M_{\text{gas}}/(\dot{M}_* L_{\text{opt}})$, where \dot{M}_* is the stellar mass loss rate per unit optical luminosity. Using the generally adapted value $\dot{M}_* = 1.5 \times 10^{-11} M_\odot \text{ yr}^{-1} L_\odot^{-1}$ (Faber & Gallagher 1976) and the optical luminosity within r_{cut} (Faber et al. 1997), we find $t_* \approx 8 \times 10^8 \text{ yr}$ in both galaxies. Therefore, stellar ejecta easily produce the observed ISM over the galaxy lifetime. The ISM is subject to radiative cooling, thermal evaporation due to the surrounding hot gas, heating by stellar winds and supernovae, and possibly to ram pressure stripping.

Ram pressure stripping. The observed X-ray centroids are within 0.5 kpc of the optical centers (limited by the *Chandra* aspect accuracy). This and the azimuthally symmetric X-ray morphology probably exclude any significant ongoing stripping. Stripping will be unimportant if the galaxies move together with their surrounding 100 kpc scale gas density enhancements.

Radiative cooling. The average cooling time of the ISM is $t_{\text{cool}} = 3M_{\text{gas}}kT/2\mu m_p L_x$. For the observed ISM parameters, we find $t_{\text{cool}} = 1.1 \times 10^8 \text{ yr}$ for NGC 4874 and $3.7 \times 10^8 \text{ yr}$ for NGC 4889, with a 10–20% uncertainty.

Stellar winds and supernovae. After 10^9 years past the burst of star formation, the average temperature of ejecta from normal stars and supernovae is $\sim 0.6 \text{ keV}$ (David, Forman, & Jones 1990). Therefore, stellar mass loss cannot be a source of heating for the ISM with $T = 1 - 1.8 \text{ keV}$.

Thermal evaporation. Following Cowie & McKee (1977), one can show that classical heat conduction through the ISM-ICM boundaries of our galaxies should be saturated. From their equation (64), we find the saturated evaporation timescales $t_{\text{evap}} \approx 3 \times 10^6 \text{ yr}$ for NGC 4874 and $\approx 2 \times 10^6$ for NGC 4889, with a 20% formal statistical uncertainty.

The timescales for radiative cooling and classical evaporation are both very short and the ISM would be destroyed quickly by either mechanism, unless the radiative cooling and the heat influx that drives evaporation balance each other. This would be achieved if the conductivity through the ICM-ISM interface is a factor of $t_{\text{cool}}/t_{\text{evap}} \approx 30 - 100$ below the classical value. A plausible reason for such a suppression is a disjoint magnetic structure of the ISM and ICM.

5.3. Thermal Balance in NGC 4874

If heat influx from the ICM does balance radiative cooling of the ISM, one expects that at each radius, the X-ray

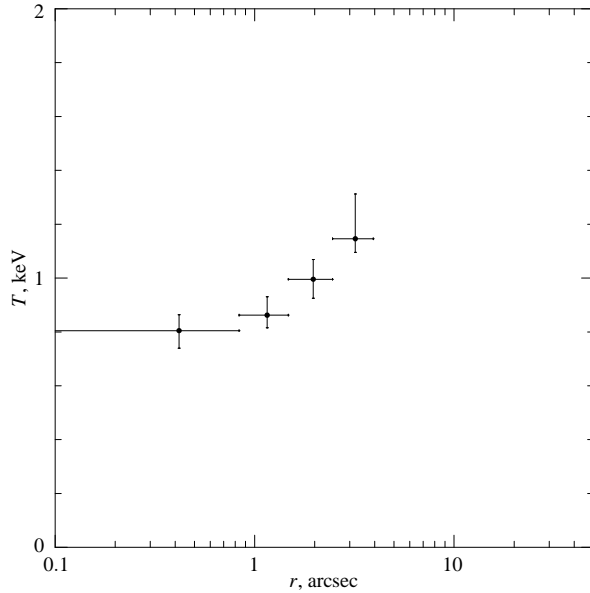


FIG. 3.— Temperature profile of NGC 4874. Metal abundance and absorption were fixed at their average values. The statistical significance of the temperature difference in the radial ranges $0''$ – $1.5''$ and $1.5''$ – $4''$ is 99%. The temperature gradient can be modeled as $T/\text{keV} = 0.87 + 0.51\lg(r/\text{arcsec})$

volume emissivity of the ISM equals the divergence of the heat flux (i.e., the local heating rate). Interestingly, this can be verified for NGC 4874, where we observe a temperature gradient and therefore can estimate the heat flux. Assuming that conductivity in the ISM is classical, the heat flux is $q = -6 \times 10^{-7} T^{5/2} dT/dr \text{ erg cm}^{-2} \text{ s}^{-1}$ where T is the plasma temperature in degrees (McKee & Cowie 1977). For the observed radial dependence of temperature in NGC 4874 which can be modeled as $T(r) = 1.0 \times 10^7 [1 + 0.71\lg(r/0.68\text{kpc})]$ (Fig. 3), the divergence of q is indeed within a factor of 1.5 of the observed X-ray volume emissivity.

For NGC 4889, the uncertainty in the temperature profile is too large to compute the heat flux. However, we can say that its ISM temperature is too high to be plausibly maintained by internal heat sources such as stellar mass loss and supernovae, so there should be external heating, most likely due to conduction through the ISM boundary.

6. SUMMARY

Chandra observations show that the dominant Coma galaxies retain a fraction of their X-ray coronae in the form of compact (~ 3 kpc in size) clouds with temperatures of 1.0 and 1.8 keV

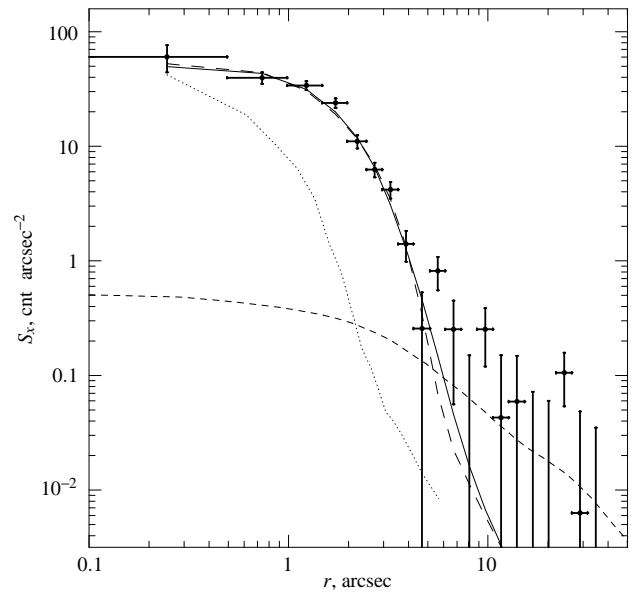


FIG. 4.— X-ray surface brightness profile of NGC 4874 in the 0.5–2 keV band. Dotted line shows the expected radial profile for a point-like source; it is consistent with the observed profile of the source located $\approx 1'$ to the East of NGC 4874 (Fig. 2). The solid line shows a β -model fit. The long-dashed line shows a β -model fit truncated at $r = 4''$. The fits are almost indistinguishable because of the PSF smearing. The dashed line shows the HST optical surface brightness profile multiplied by the observed ratio $L_{\text{LMXB}}/L_{\text{opt}}$ (Sarazin et al. 2000) and therefore should represent the LMXB contribution to the observed X-ray flux.

which are in the pressure equilibrium with the hot intracluster gas. Time scales for radiative cooling and classical evaporation are very short but the ISM observed in two galaxies is unlikely to be a transient phenomenon. We propose that cooling in the ISM is balanced by heat influx through the cluster/ISM interface. For this, thermal conductivity through the interface should be 30–100 times below the classical value, perhaps because of the disjoint magnetic field structure. Furthermore, in NGC 4874, the observed radial temperature gradient implies that if the conductivity *inside* the ISM cloud is classical, then heat from outside the cloud is distributed through the cloud volume in such a way that it precisely balances radiative cooling at each radius. This leaves little or no energy for the ISM evaporation, preserving the ISM clouds for a sufficiently long time.

We thank E. Churazov for useful discussions. The financial support for this work was provided by NASA grant NAG5-9217 and contract NAS8-39073.

REFERENCES

- Arnaud, M., et al. 2001, *A&A*, 365, L67
 Balbus, S. A. & McKee, C. F. 1982, *ApJ*, 252, 529
 Bandiera, R. & Chen, Y. 1994, *A&A*, 284, 637
 Bechtold, J., Forman, W., Giacconi, R., Jones, C., Schwarz, J., Tucker, W., & Van Speybroeck, L. 1983, *ApJ*, 265, 26
 Böhringer, H. & Fabian, A. C. 1989, *MNRAS*, 237, 1147
 Briel, U. G., Henry, J. P., & Böhringer, H. 1992, *A&A*, 259, L31
 Briel, U. G., et al. 2001, *A&A*, 365, L60
 Cowie, L. L. & McKee, C. F. 1977, *ApJ*, 211, 135
 David, L. P., Forman, W., & Jones, C. 1990, *ApJ*, 359, 29
 Faber, S. & Gallagher, J. 1976, *ApJ*, 204, 365
 Faber, S. M. et al. 1997, *AJ*, 114, 1771
 Fabian, A. C. 1994, *ARA&A*, 32, 277
 Fabian, A. C., Canizares, C. R., & Böhringer, H. 1994, *ApJ*, 425, 40
 Forman, W., Jones, C., & Tucker, W. 1985, *ApJ*, 293, 102.
 McKee, C. F. & Begelman, M. C. 1990, *ApJ*, 358, 392
 McKee, C. F. & Cowie, L. L. 1977, *ApJ*, 215, 213
 Sarazin, C. L., Irwin, J. A., & Bregman, J. N. 2001, *ApJ*, submitted
 Vikhlinin, A., Forman, W., & Jones, C. 1994, *ApJ*, 435, 162
 Vikhlinin, A., Forman, W., & Jones, C. 1997, *ApJ*, 474, L7
 White, S. D. M., Briel, U. G., & Henry, J. P. 1993, *MNRAS*, 261, L8